PROCEEDINGS OF SPIE

Lower jawbone data generation for deep learning tools under MeVisLab

Birgit Pfarrkirchner, Christina Gsaxner, Lydia Lindner, Norbert Jakse, Jürgen Wallner, et al.

SPIE.

Lower Jawbone Data Generation for Deep Learning Tools under MeVisLab

Birgit Pfarrkirchner[a,b], Christina Gsaxner[a,b], Lydia Lindner[a,b], Norbert Jakse[c], Jürgen Wallner[b,c]
Dieter Schmalstieg[a] and Jan Egger[a,b,d]

[a] TU Graz, Institute for Computer Graphics and Vision (ICG), Inffeldgasse 16c/II, 8010 Graz, Styria, Austria
[b] Computer Algorithms for Medicine (Cafe) Laboratory, 8010 Graz, Styria, Austria
[c] Department of Maxillofacial Surgery, Medical University of Graz, Auenbruggerplatz 12, 8036 Graz, Styria, Austria
[d] BioTechMed-Graz, Krenngasse 37/1, 8010 Graz, Styria, Austria

ABSTRACT

In this contribution, the preparation of data for training deep learning networks that are used to segment the lower jawbone in computed tomography (CT) images is proposed. To train a neural network, we had initially only ten CT datasets of the head-neck region with a diverse number of image slices from the clinical routine of a maxillofacial surgery department. In these cases, facial surgeons segmented the lower jawbone in each image slice to generate the ground truth for the segmentation task. Since the number of present images was deemed insufficient to train a deep neural network efficiently, the data was augmented with geometric transformations and added noise. Flipping, rotating and scaling images as well as the addition of various noise types (uniform, Gaussian and salt-and-pepper) were connected within a global macro module under MeVisLab. Our macro module can prepare the data for general deep learning data in an automatic and flexible way. Augmentation methods for segmentation tasks can easily be incorporated.

Keywords: Data Augmentation, Lower Jawbone, MeVisLab, Deep Learning, Medical Image Segmentation, Computed Tomography (CT).

1. DESCRIPTION OF PURPOSE

Segmentation is an important branch in medical image processing and the basis for further detailed investigations on computed tomography (CT), magnetic resonance imaging (MRI), X-ray, ultrasound (US) or nuclear images [1]-[8]. Through segmentation, an image is divided into various connected areas that correspond to certain tissue types. A common aim is to delineate healthy and pathologic tissues. A frequent example in medicine is the identification of a tumor or pathological lesion and its volume to evaluate treatment planning and outcome [9]-[15]. In the clinical routine, segmentation is necessary for the planning of specific treatment tasks [16]-[20], that are for example used in the radiation therapy or for the creation of three-dimensional (3D) visualizations and models to simulate a surgical procedure [21]-[23]. Segmentation can be classified into several families of techniques, such as thresholding [24], region growing, watershed [25], edge-based approaches, active contours [26] and model-based algorithms [27]. Recently, deep learning using neural networks is becoming important for automatic segmentation applications [28], [29].

Neural networks are constructed of neurons that are organized into input layers, output layers, and hidden layers, which are located between the input and output layers. Neural networks with a large number of layers are known as deep networks. The neurons are connected via weights, which can be trained with a training dataset to solve specific problems. For efficient training, neural networks require large amounts of training data [30], [31]. However, there is a lack of medical images that can be used as training data, because a ground truth data set has to be generated in advance by a physician through the manual segmentation of each slice. Moreover, medical images from the clinical routine need approval for research usage and must be anonymized, which may be a limiting factor.

An opportunity to generate more training data from a small set of original images is data augmentation [30]-[33]: The original images are, for instance, geometrically transformed; random noise is added, or the resolution is changed. Augmentation is a common method in deep learning research [34], [35], [36].

To train deep learning networks for lower jawbone (mandible) segmentation, we used anonymized CT datasets from ten patients of the complete head and neck region. All CT data acquisitions have been performed in the clinical routine for diagnostic reasons at a maxillofacial surgery department at our disposal. Each mandible of these CT images was segmented by two specialized doctors manually (slice-by-slice in axial direction) to generate the ground truth contours for the segmentation task. To increase this rather small number of images, we resorted to data augmentation using the image processing platform MeVisLab (http://www.mevislab.de/download/). The segmentation contours were initially

exported as contour segmentation objects (CSO) and voxelized for training a neural network. The single transverse slices of the segmentation mask that covered the mandibular and the corresponding original slices were saved separately.

2. METHODS

All implementations of this work were accomplished with the MeVisLab platform [37]-[42]. MeVisLab is a medical image processing software with a graphical user interface. Besides, it provides built-in modules for basic image processing operations, such as low-pass filtering. These modules can be connected to form image processing networks [43]-[49].

We developed a MeVisLab module network (Figure 1) that converts segmentation contours into ground truth images and a depiction of the patients' CT images. In addition, a MeVisLab macro module was created, which saves image data as separate and, optionally, modified slices.

At the lower section of the network is the *Load Data* module group (green box in Figure 1) to import the patient's CT dataset and the segmentation contours of the lower jawbone into the MeVisLab environment. The *CSOConvertToImage* module (orange box in Figure 1) converts a CSO into a voxelized ground truth binary mask (Figure 2). The modules at the top of Figure 1 display the CT images and masks.

In addition, we developed a *SaveAsSingleSlices* (red box in Figure 1) macro-module, which allows storing all slices of one image data stack as separate TIFF or PNG files automatically. In addition, our macro-module is able to export selected slices and to augment the dataset with geometric transformations and noise. Geometric transformations may use any combination of rotation, scaling and mirroring, while noise can be of the uniform, Gaussian or salt-and-pepper variety. All parameters can be interactive specified in a custom user interface panel.
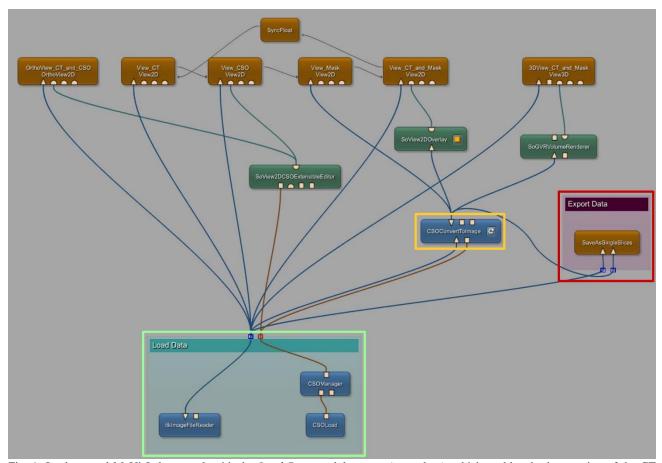

Fig. 1: Implemented MeVisLab network with the *Load Data* module group (green box), which enables the importation of the CT images and the CSO files. The *CSOConvertToImage* module (orange box) converts the contours into binary images. Finally, the generated *SaveAsSingleSlices* (red box) module enables the automatic exportation of the image slices and the application of data augmentation methods.
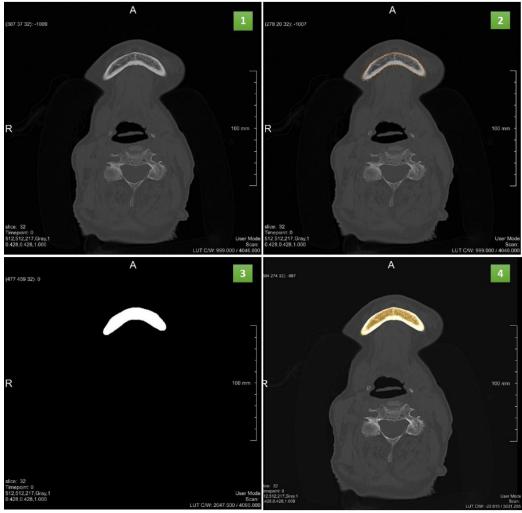
Fig. 2: Various representations created with a View2D modules. No. 1 shows the original CT, No. 2 the CT with an overlaid contour, No. 3 the binary mask and No. 4 the CT with the overlaid binary mask.

3. RESULTS

The number of exportable images relies on the definition of the storage parameters by the user. If the default values for transformation and adding noise are applied on a single slice, it is possible to export eleven slices (the original slice and ten artificially generated slices). We chose rotation angles of $\pm 8°$, and a scale of 1 ± 0.04 in x- and y-direction. The amplitude of uniform noise has a value of 800 gray values, the Gaussian noise has a mean value of zero and a standard deviation of 300 gray values. The salt-and-pepper amplitudes are set to ±2000 gray values, and the density is set to a value of 0.05.

All settings can be modified depending on the user's intention. Thus, arbitrary training data sets can be produced – for the standard parameter setting, we could blow up our 1680 images with a ground truth segmentation to 18,480 images with corresponding ground truth segmentations. However, it must be kept in mind that the settings should produce images that are physiologically meaningful. Since clinical CT data is mostly acquired in supine position, a rotation by more than a few degrees is not meaningful for the most tasks [50]. Figure 3 displays an original CT slice and two artificially generated images based on the original image. Finally, the code is freely available for download [51]:

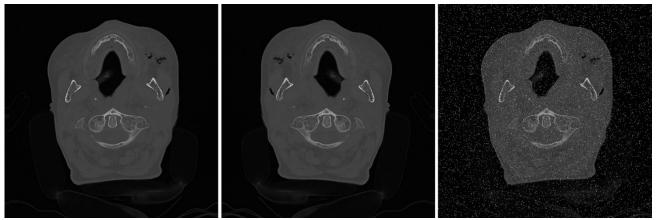https://github.com/birgitPf/Data_Generation

Fig. 3: Examples of exported CT slices in the lower jawbone area. The left image shows the original acquired CT slice of a patient. In the middle, is a flipped version of the left image visible. The right CT slice displays an image with added salt-and-pepper noise (amplitude ± 2000 and density 0.05).

4. CONCLUSIONS

In this work, a MeVisLab network and a macro-module have been developed to provide a convenient way to handle data preparation and augmentation for the segmentation of the lower jawbones with deep learning networks. The macro-module provides a convenient interface for tuning the training data set by selecting slices and applying freely configurable data augmentation. This approach makes it easy to systematically vary the data set before training.

The current implemented methods are already suitable for creating augmented data sets to train neural networks for automatic segmentation tasks. However, if more data is necessary, it is possible to extend our existing MeVisLab module with further functions for data augmentation, such as elastic deformations, shearing or translation.

ACKNOWLEDGEMENT

REFERENCES

[1] Egger, J. et al. "Interactive-cut: Real-time feedback segmentation for translational research," Computerized Medical Imaging and Graphics 38 (4), 285-295 (2014).

[2] Egger, J. et al. "PCG-Cut: Graph Driven Segmentation of the Prostate Central Gland," PLOS ONE 8 (10), e76645 (2013).

[3] Egger, J. et al. "Preoperative Measurement of Aneurysms and Stenosis and Stent-Simulation for Endovascular Treatment," IEEE International Symposium on Biomedical Imaging: From Nano to Macro, Washington (D.C.), USA, pp. 392-395, IEEE Press (2007).

[4] Egger, J. "Refinement-Cut: User-Guided Segmentation Algorithm for Translational Science," Sci Rep 4:5164 (2014).

[5] Zukic, D. et al. "Robust Detection and Segmentation for Diagnosis of Vertebral Diseases using Routine MR Images," Computer Graphics Forum, Volume 33, Issue 6, Pages 190–204 (2014).

[6] Zukic, D. et al. "Segmentation of Vertebral Bodies in MR Images," Vision, Modeling, and Visualization (VMV), The Eurographics Association, pp. 135-142, (2012).

[7] Bauer, M. et al. "A fast and robust graph-based approach for boundary estimation of fiber bundles relying on fractional anisotropy maps," 20th International Conference on Pattern Recognition (ICPR), Istanbul, Turkey, pp. 4016-4019 (2010).

[8] Bauer, M. et al. "Boundary estimation of fiber bundles derived from diffusion tensor images," International journal of computer assisted radiology and surgery 6 (1), 1-11 (2011).

[9] Egger, J. et al. "GBM Volumetry using the 3D Slicer Medical Image Computing Platform," Sci Rep., Nature Publishing Group (NPG), 3:1364 (2013).

[10] Egger, J. et al. "Simulation of bifurcated stent grafts to treat abdominal aortic aneurysms (AAA)," Proceedings of SPIE Medical Imaging Conference, Vol. 6509, pp. 65091N(1-6), San Diego, USA (2007).

[11] Egger, J. et al. "Fast self-collision detection and simulation of bifurcated stents to treat abdominal aortic aneurysms (AAA)," 29th Annual International Conference of the IEEE Engineering in Medicine and Biology Society, Lyon, France, pp. 6231-6234, IEEE Press (2007).

[12] Egger, J. et al. "Pituitary Adenoma Volumetry with 3D Slicer," PLOS ONE 7 (12), e51788 (2012).

[13] Egger, J. et al. "Nugget-Cut: A Segmentation Scheme for Spherically- and Elliptically-Shaped 3D Objects," 32nd Annual Symposium of the German Association for Pattern Recognition (DAGM), LNCS 6376, pp. 383–392, Springer Press, Darmstadt, Germany (2010).

[14] Egger, J. et al. "Template-Cut: A Pattern-Based Segmentation Paradigm," Sci Rep 2:420 (2012).

[15] Egger, J. et al. "Interactive Volumetry of Liver Ablation Zones," Sci Rep 5:15373 (2015).

[16] Egger, J. et al. "Aorta Segmentation for Stent Simulation," 12th International Conference on Medical Image Computing and Computer Assisted Intervention (MICCAI), Cardiovascular Interventional Imaging and Biophysical Modelling Workshop, 10 pages, London, UK (2009).

[17] Egger, J. et al. "Graph-Based Tracking Method for Aortic Thrombus Segmentation," Proceedings of 4th European Congress for Medical and Biomedical Engineering, Engineering for Health, Antwerp, Belgium, Springer, pp. 584-587 (2008).

[18] Renapurkar, R. D. et al. "Aortic volume as an indicator of disease progression in patients with untreated infrarenal abdominal aneurysm," European Journal of Radiology 81 (2012) e87–e93 (2012).

[19] Egger, J. et al "A flexible semi-automatic approach for glioblastoma multiforme segmentation," Proceedings of International Biosignal Processing Conference, Charité, Berlin, Germany (2010).

[20] Egger, J. et al. "Pituitary Adenoma Segmentation," In: Proceedings of International Biosignal Processing Conference, Charité, Berlin, Germany (2010).

[21] Chen, X. et al. "Development of an open source software module for enhanced visualization during MR-guided interstitial gynecologic brachytherapy," SpringerPlus, 3:167 (2014).

[22] Egger, J. "Image-guided therapy system for interstitial gynecologic brachytherapy in a multimodality operating suite," SpringerPlus, 2:395 (2013).

[23] Egger, J., Mostarkic, Z., Grosskopf, S. and Freisleben, B. "A Fast Vessel Centerline Extraction Algorithm for Catheter Simulation," 20th IEEE International Symposium on Computer-Based Medical Systems, Maribor, Slovenia, pp. 177-182, IEEE Press (2007).

[24] Sezgin, M. and Sankur, B. "Survey over image thresholding techniques and quantitative performance evaluation," J. Electron. Imaging, 13(1):146-168 (2004).

[25] Bleau, A. and Leon, J. L. "Watershed-Based Segmentation and Region Merging," Computer Vision and Image Understanding, 77(3):317-370 (2000).

[26] Lu, J. et al. "Detection and visualization of endoleaks in CT data for monitoring of thoracic and abdominal aortic aneurysm stents," Proc. of SPIE Vol 6918, 69181F-1 (2016).

[27] Greiner, K. et al. "Segmentation of Aortic Aneurysms in CTA Images with the Statistic Approach of the Active Appearance Models," Proceedings of Bildverarbeitung für die Medizin (BVM), Berlin, Germany, Springer Press, 51-55 (2008).

[28] Handels, H. "Medizinische Bildverarbeitung Bildanalyse, Mustererkennung und Visualisierung für die computergestützte ärztliche Diagnostik und Therapie," Wiesbaden: Vieweg + Teubner (2006).

[29] Bankman, I. N. and Rogowska, J. "Handbook of Medical Image Processing and Analysis," Burlington (USA): Academic Press - Elsevier, 71-90 (2009).

[30] Suk, H.-I. "An Introduction to Neural Networks and Deep Learning," in Deep Learning for Medical Image Analysis, London, Academic Press - Elsevier, 3-24 (2017).

[31] Srinivas, S. et al. "An Introduction to Deep Convolutional Neural Nets for Computer Vision," in Deep Learning for Medical Image Analysis, London, Academic Press - Elsevier, 25-52 (2017).

[32] Christlein, V. and Würfl, T. "Deep Learning Tutorial - Basics," DKFZ, Heidelberg, 1-90 (2017).

[33] Lindner, L. & Egger, J. "Artificial Brain Tumor Data Generation for Deep Learning Based Segmentation Approaches," Technical Report, Graz University of Technology, pp. 1-39 (2017).

[34] Simard, P. Y. "Best Practices for Convolutional Neural Networks Applied to Visual Document Analysis," in Proceedings of the Seventh International Conference on Document Analysis and Recognition - Volume 2, Washington (2003).

[35] Chatfield, K. et al. "Return of the Devil in the Details: Delving Deep into Convolutional Nets," in Proceedings of the British Machine Vision Conference, Nottingham (2014).

[36] Krizhevsky, A. et al. "ImageNet Classification with Deep Convolutional Neural Networks," in Advances in Neural Information Processing Systems 25 (2012).

[37] Egger, J. et al. "Integration of the OpenIGTlink network protocol for image guided therapy with the medical platform MeVisLab," The international Journal of medical Robotics and Computer assisted Surgery, 8(3):282-390 (2012).

[38] Kuhnt, D. et al. "Fiber tractography based on diffusion tensor imaging (DTI) compared with High Angular Resolution Diffusion Imaging (HARDI) with compressed sensing (CS) – initial experience and clinical impact," Neurosurgery, Volume 72, pp. A165-A175 (2013).

[39] Gsaxner, C. et al. "Exploit 18F-FDG Enhanced Urinary Bladder in PET Data for Deep Learning Ground Truth Generation in CT Scans," SPIE Medical Imaging (2018).

[40] Gsaxner, C. & Egger, J. "Preparation of Training Data for automatic Urinary Bladder Segmentation using Deep Learning," Technical Report, Graz University of Technology, May 2017, pp. 1-35 (2017).

[41] Gsaxner, C. & Egger, J. "MeVisLab Macro Module for Preparation of Training Data for Urinary Bladder Segmentation," GitHub (2017).

[42] Egger, J. et al. "HTC Vive MeVisLab integration via OpenVR for medical applications," PLoS ONE 12(3): e0173972 (2017).

[43] Schwarzenberg, R. et al. "A Cube-Based Approach to Segment Vertebrae in MRI-Acquisitions," Proceedings of Bildverarbeitung für die Medizin (BVM), Springer Press, pp. 69-74 (2013).

[44] Schwarzenberg, R. et al. "Cube-Cut: Vertebral Body Segmentation in MRI-Data through Cubic-Shaped Divergences," In: PLoS One (2014).

[45] Egger, J. et al. "A medical software system for volumetric analysis of cerebral pathologies in magnetic resonance imaging (MRI) data," Journal of medical systems 36 (4), 2097-2109 (2012).

[46] Egger, J. et al. "Modeling and Visualization Techniques for Virtual Stenting of Aneurysms and Stenoses," Computerized Medical Imaging and Graphics, 36(3), pp. 183-203 (2012).

[47] Egger, J. et al. "Manual refinement system for graph-based segmentation results in the medical domain," Journal of medical systems 36 (5), 2829-2839 (2012).

[48] Gall, M., et al. "Computer-Aided Planning and Reconstruction of Cranial 3D Implants," IEEE Engineering in Medicine and Biology Society (EMBC'16), Orlando, FL, August USA, IEEE Press, pp. 1179-1183 (2016).

[49] Gall, M. et al. "Computer-Aided Planning of Cranial 3D Implants," Int J CARS 11 (Sup. 1):S241, Heidelberg, Germany (2016).

[50] Pfarrkirchner, B. & Egger, J. "Generation of data for Deep Learning tools," Technical Report, Graz University of Technology, May 2017, pp. 1-58 (2017).

[51] Pfarrkirchner, B. & Egger, J. "Lower Jawbone Data Generation for Deep Learning Tools under MeVisLab," GitHub (2017).